Coordination of SMES, SFCL and Distributed Generation Units for Micro-Grid Stability Enhancement via Wireless Communications

**LEI CHEN[ID]1, (Member, IEEE), HONGKUN CHEN1, GUOCHENG LI[ID]1, XIN TIAN[ID]2,
YING XU[ID]3, (Member, IEEE), LI REN[ID]3, (Senior Member, IEEE), YANHONG LI4,
LIN ZHU5, (Member, IEEE), AND YUEJIN TANG3**

[1] School of Electrical Engineering, Wuhan University, Wuhan 430072, China
[2] School of Electronic Information, Wuhan University, Wuhan 430072, China
[3] State Key Laboratory of Advanced Electromagnetic Engineering and Technology, Huazhong University of Science and Technology, Wuhan 430074, China
[4] Guangzhou Power Supply Company Ltd., China Southern Power Grid Company Ltd., Guangzhou 510620, China
[5] Department of Electrical Engineering and Computer Science, The University of Tennessee, Knoxville, TN 37996, USA

Corresponding author: Lei Chen (stclchen1982@163.com)

ABSTRACT To enhance the stability of a micro-grid under fault conditions, this paper proposes the coordination control of a superconducting magnetic energy storage (SMES), an active superconducting fault current limiter (SFCL), and distributed generation units via wireless network communications. This coordination control can smoothly separate the micro-grid from the main network in the case of severe or permanent faults, and assist the micro-grid to achieve the fault ride-through (FRT) operation if the fault is minor or temporary. Details on the modeling, control strategy, and network architecture are presented. Moreover, the simulation analysis of a 10-kV class micro-grid including the SMES, SFCL, and photovoltaic generation units is implemented in MATLAB. Concerning the performance evaluation of the coordination control not only the severe and minor faults but also different communication delays are taken into account. The results confirm the effectiveness of the proposed coordination control.

INDEX TERMS Coordination control, distributed generation, micro-grid, superconducting fault current limiter (SFCL), superconducting magnetic energy storage (SMES), wireless communications.

NOMENCLATURE

FRT	Fault ride-through.
SFCL	Superconducting fault current limiter.
SMES	Superconducting magnetic energy storage.

SYMBOLS

i	Current [A].
L	Inductance [H].
M	Mutual inductance [H].
P	Power [W].
Z	Impedance [Ω].
v	Voltage [V].
X	Reactance [Ω].
ω	Angular velocity [rad/s].

SUBSCRIPTS

g	Grid.
f	Fault.
d	d-axis.
q	q-axis.
n	Nominal.
pv	Photovoltaic.
dc	Direct current.
$s1$	Superconducting transformer's primary coil.
$s2$	Superconducting transformer's secondary coil.
pcc	Point of common coupling.
vsc	Voltage source converter.

I. INTRODUCTION

In regards to the use of superconducting power devices in electric power systems, superconducting magnetic energy storage (SMES) and superconducting fault current

limiter (SFCL) are two representatives, and both of them have great potentials to enhance power system stability [1], [2]. SMES and SFCL can be deployed not only in high-voltage main networks, but also in low-voltage micro-grids [3]–[5], which are usually to integrate and maximize the utilization of distributed generation units. Due to continuous increasing penetration levels and power exchanges, it is crucial to guarantee the stability of a high penetration micro-grid, especially when short-circuit faults occur. Actually, for that a micro-grid should transfer to the island mode from the original grid-connected mode in case of a severe fault, there are some critical challenges existing for the micro-grid's stable operation, such as a relatively low system inertia to deal with the power unbalance. Therefore, it is essential to carry out an effective voltage and frequency regulation in the event of that the micro-grid operates in the island mode, otherwise, the deviations in the micro-grid's voltage and frequency may be out of the tolerance range along with the increase of the power unbalance.

Respect to this issue, introducing a SFCL for the micro-grid enables to limit the fault current and mitigate the voltage sag when the micro-grid is under the progress of the mode transfer, and at the moment of the island mode being achieved, the fault current surge can be decreased, and the recovery process of the micro-grid voltage may be accelerated. Further, using a SMES for the micro-grid is to offer the subsequent active and reactive power compensation, and it can provide the references of voltage and frequency to stabilize the micro-grid's performance behaviors. From this viewpoint, the combined use of SMES and SFCL could provide better micro-grid control capability by taking advantage of strengths of the both devices.

A brief literature review on the micro-grid's stability and the combined use of SMES and SFCL is given as follows. In [6] and [7], the stability indexes such as clearing time and frequency grid code violation time are defined, and the small-signal stability analysis is performed for a micro-grid. In [8] and [9], a fault ride-through (FRT) control strategy and a low-pass-based damping method are proposed for the stability improvement of a micro-grid, but the performances of the two software solutions highly rely on the converter's capability. In [10], a distribution static synchronous compensator is introduced as a hardware solution; however, its effectiveness under some severe fault conditions can be further improved. In [11]–[13], the combined use of SMES and SFCL in a traditional power grid with a wind farm has been validated, but few details are related to a micro-grid. Our research group has preliminarily conducted the coordination study of a flux-coupling type SFCL and a SMES for a micro-grid [14]. Although this technical idea has been proved feasible, the preliminary study has not addressed the distributed generation coordinated action and the data communication architecture. In addition, using a SFCL based-power-electronics may be more preferable to achieve a more efficient coordination among SMES, SFCL and distributed generation units.

In this paper, a feasible coordination control of the SMES, SFCL and multiple distributed generation units is proposed for a micro-grid, and it is expected to enhance the micro-grid's robustness against short-circuit faults. Specifically, a voltage compensation type active SFCL is selected, and the utilization of wireless network communications as well as the difference of fault severities are investigated.

II. THEORETICAL ANALYSIS

From FIGURE 1, the micro-grid includes a SMES unit, an active SFCL, two solar PV generators, and two static power loads. A coordinated control center is configured, and here a bidirectional data exchange with SMES/SFCL/distributed generation units and a unidirectional data exchange with loads can be achieved using the wireless network.
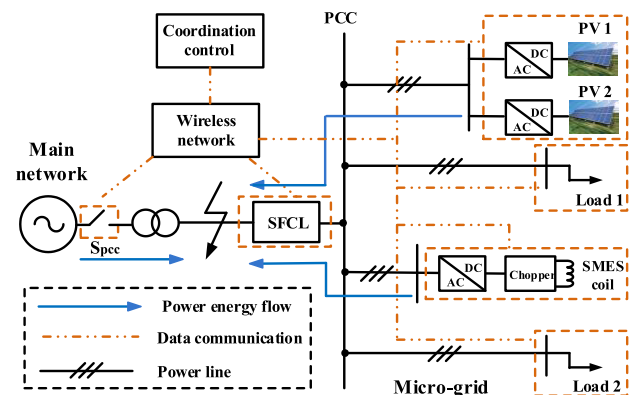

FIGURE 1. Schematic diagram of a micro-grid with SMES, SFCL and distributed generation units.

A. MODELING, CONTROL, AND DESIGN OF THE SMES

Compared to other types of energy storage devices, the selection of SMES can offer the following technical advantages: fast response, high efficiency, high energy density, great controllability and unlimited number of charging and discharging cycles, and introducing a SMES for a micro-grid can contribute to controlling the constant power flow at the point of common coupling (PCC), frequency, and voltage of the micro-grid [3], [4], [15]. A SMES unit mainly consists of three parts: voltage source converter, a direct-current chopper circuit, and a superconducting magnet [16]. FIGURE 2 shows the control diagram of the SMES. When the micro-grid is normally connected to the main network, the SMES operates in the active and reactive power control (P-Q control) mode to achieve an expected power tracking [17]. The voltage source converter's mathematical model is expressed as:

$$\begin{cases} Ldi_d/dt = e_d + \omega Li_q - v_{dc}s_d \\ Ldi_q/dt = e_q - \omega Li_d - v_{dc}s_q \end{cases} \quad (1)$$

where i, e denotes the current and voltage, respectively; s is the control signal; subscripts d and q indicate the d-axis and the q-axis, respectively; v_{dc} is the voltage over the converter's
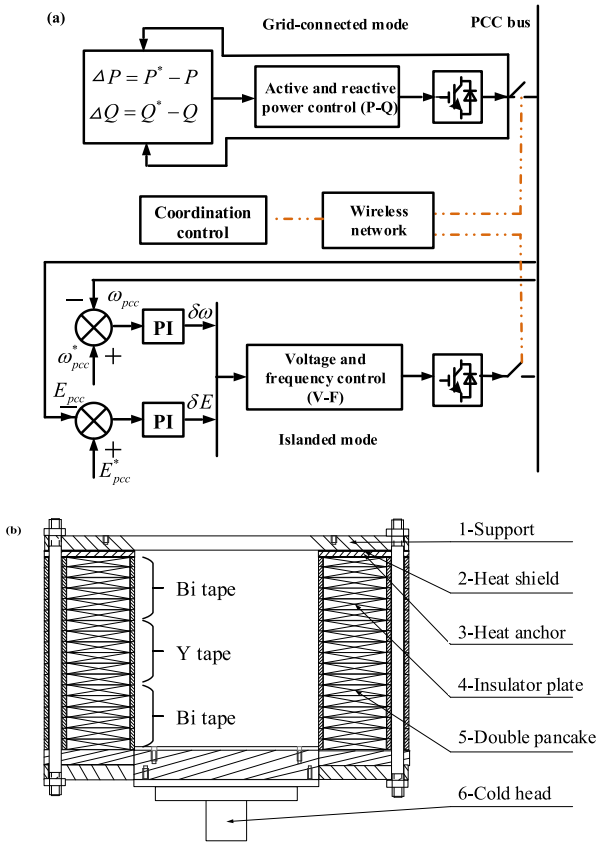
FIGURE 2. (a) Control block diagram of the SMES. (b) Schematic structure diagram of the superconducting magnet.

DC side; L is a connecting inductance. Thus, the current control equation of the voltage source converter can be expressed as:

$$\begin{cases} v_{vsc\_d\_ref} = (K_p + K_i/s)(i_{d\_ref} - i_d) + e_d - \omega L i_q \\ v_{vsc\_q\_ref} = (K_p + K_i/s)(i_{q\_ref} - i_q) + \omega L i_d \end{cases} \quad (2)$$

where K_p, K_i are the given proportional and integral parameters of the current regulator, respectively; $v_{vsc-d-ref}$ and $v_{vsc-q-ref}$ are the d-axis and q-axis voltage references of the voltage source converter, respectively.

When the micro-grid switches to its islanded mode, the voltage-frequency (V-F) control of the SMES will be activated to stabilize the micro-grid. Here, the voltage deviation δE and the frequency deviation $\delta \omega$ are calculated, and then they will be sent to the V-F control regulator for production of the driving signals. From FIGURE 2 (a), the control transfer between the P-Q and the V-F modes is handled by the coordinated control center.

Considering that the micro-grid is generally connected to the distribution network, the power exchange can be as high as several kW to several MW, and the characteristics of the micro-grid are quite different from those of a high-voltage power transmission grid. Thus, it is recommended to introduce the SMES and meanwhile to consider its techno-economics. In a sense, the design of the superconducting

magnet is critical. According to the two kinds of super-conducting tapes from our lab, a preliminary design of the superconducting magnet is explored. Based on the product manual, the BSCCO tape (4.5 mm width × 0.36 mm height, $I_c = 180$ A) is made by Sumitomo Electric, and the YBCO tape (4.8 mm width × 0.2 mm height, $I_c = 90$ A) is made by AMSC. FIGURE 2(b) shows the schematic structure diagram of the superconducting magnet, which is treated as a hybrid magnet including both BSCCO and YBCO tapes. From the designed structure, the coils wound by the BSCCO tapes are arranged for the head and end of the magnet, and the coils wound by the YBCO tapes are arranged for the middle of the magnet. Under this arrangement, the hybrid superconducting magnet may have a high critical current and sufficient current margin [18], [19], so as to enhance its technical and economic properties to a certain extent.

B. MODELING, CONTROL, AND DESIGN OF THE ACTIVE SFCL

FIGURE 3(a) indicates the electrical configuration of a voltage compensation type active SFCL (single-phase connection) [20]. This recommended active SFCL is mainly composed of three parts, an air-core superconducting transformer, a voltage-type pulse-width-modulation (PWM) converter, and a LC filter. For the SFCL using superconductors and power electronics, its working philosophy is to control
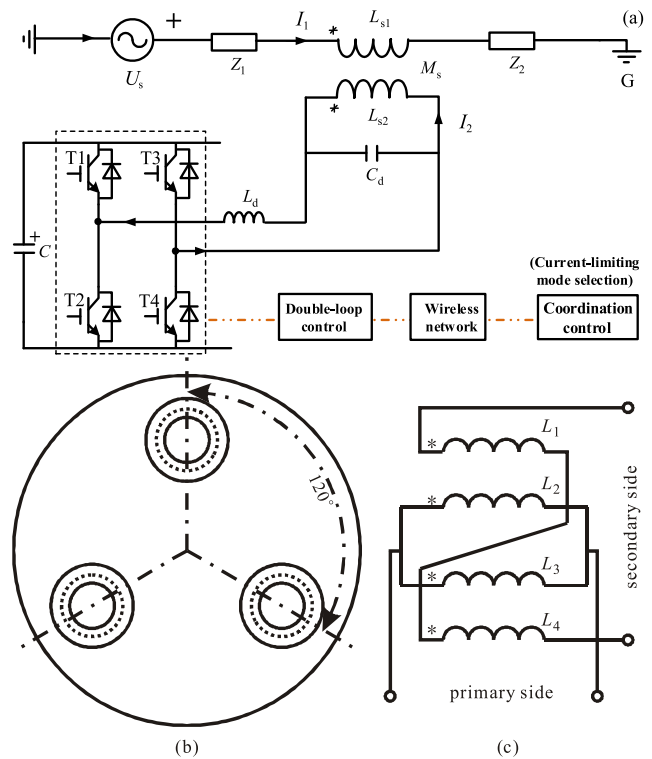

FIGURE 3. (a) Schematic diagram of a voltage compensation type active SFCL. (b) Layout diagram of three individual single-phase superconducting transformers. (c) Winding arrangement of a single-phase superconducting transformer.

the current (I_2) flowing in the secondary winding of the air-core transformer by the converter.

In normal condition, adjusting I_2 is to make the impedance $Z_{SFCL} = 0$, and using the active SFCL will not affect the relevant system. Under fault condition (Z_2 is shorted to do the current-limiting analysis), the main current will rise from I_1 to I_{1f}, and the primary voltage will increase to U_{1f}.

$$\dot{I_{1f}} = (\dot{U}_s + j\omega M_s \dot{I_2})/(Z_1 + j\omega L_{s1}) \tag{3}$$

$$\begin{aligned} \dot{U_{1f}} &= j\omega L_{s1}\dot{I_{1f}} - j\omega M_s \dot{I_2} \\ &= \frac{\dot{U}_s(j\omega L_{s1}) - \dot{I_2}Z_1(j\omega M_s)}{Z_1 + j\omega L_{s1}} \end{aligned} \tag{4}$$

The current-limiting impedance Z_{SFCL} is expressed as [21]:

$$Z_{SFCL} = \frac{\dot{U_{1f}}}{\dot{I_{1f}}} = j\omega L_{s1} - \frac{j\omega M_s \dot{I_2}(Z_1 + j\omega L_{s1})}{\dot{U}_s + j\omega M_s \dot{I_2}} \tag{5}$$

As the amplitude value and phase angle of the current I_2 can be regulated, three current-limiting modes are basically set:

1) Making I_2 remain the original status, $Z_{SFCL-1} = Z_2(j\omega L_{s1})/(Z_1 + Z_2 + j\omega L_{s1})$.

2) Controlling $I_2 = 0$, $Z_{SFCL-2} = j\omega L_{s1}$.

3) Regulating the phase angle of I_2 to make the angle difference between $\dot{U}_s$ and $j\omega M_s \dot{I_2}$ be 180°, $Z_{SFCL-3} = cZ_1/(1-c) + j\omega L_{s1}/(1-c)$ is obtained, where the variable c is defined by $j\omega M_s \dot{I_2} = -c\dot{U}_s$.

The coordinated center selects a current-limiting mode for the SFCL, and the selection result will be sent to the controller of the converter by the wireless network. In this study, the converter uses a double-loop control strategy [21], including an outer loop for voltage control and an inner loop for current control. After a series of computations from the referenced signals, the pulse signals are produced to drive the PWM converter.

It should be noted that, the active SFCL is used to suppress the fault current and compensate the voltage sag before the micro-grid is separated from the point of common coupling. The active SFCL offers the following performance advantages: 1) High controllability and flexibility due to the converter. Compared to a simple resistive or inductive SFCL, the active SFCL owns multiple current-limiting modes, and its impedance Z_{SFCL} can be flexibly controlled in terms of different current-limiting requirements. It means that the active SFCL has the abilities of controlling the fault current and compensating the voltage sag within the expected ranges. In particular, the active SFCL's impedance Z_{SFCL} under its current-limiting mode 3 can offer both of resistive and inductive components, and this technical character is helpful to more effectively dissipate the surplus active power and mitigate the power oscillation during the grid faults. 2) Great applicability for different voltage levels owing to the adjustment of the transformer. 3) Excellent linearity of Z_{SFCL} thanks to avoiding the magnetic saturation in the air-core. In addition, there is no iron loss in the air-core superconducting transformer, which may have a comprehensive

reduction in the size, weight and harmonic in comparison to a conventional iron-core superconducting transformer [22]. In summary, introducing the active SFCL in the micro-grid offers good potentials for responding to the control commands and participating in the coordinated operation.

Concerning the design of the active SFCL in the micro-grid, a possible structure of the air-core superconducting transformer is presented. By use of a simplified way, three individual single-phase air-core superconducting transformers are adopted for their applications in a three-phase type micro-grid. FIGURE 3(b) shows the layout diagram, which is helpful to alleviate the phase-to-phase flux disturbance and save the cooling cost as much as possible [23], [24]. FIGURE 3(c) indicates the winding arrangement of the single-phase superconducting transformer, whose primary and secondary windings include one or more double pancakes. This staggered arrangement can enhance the superconducting transformer's coupling coefficient and reduce the initial current flowing in the secondary winding [25]. In addition, it is pointed out that the three current-limiting modes provide different capacity demands for the pulse-width-modulation converter, but the main part of Z_{SFCL} is theoretically determined by the superconducting transformer.

C. CONFIGURATION AND CONTROL OF THE PV UNIT

FIGURE 4 indicates the configuration structure of a PV generation unit connected to the micro-grid. Under normal condition, the boost converter will adopt the maximum power point tracking control to guarantee the PV efficiency. The transistors $V_{T1} \sim V_{T6}$ are used to denote the insulated gate bipolar transistors. According to FIGURE 4, the power equation can be conducted as:

$$P_{PV} = P_{DC1} + P_g \tag{6}$$

where P_{DC1} is the power stored in the DC-link capacitor C_1; P_g is the transmission power from the inverter to the micro-grid; P_{PV} is expressed as the PV array output. For the loss of the converter is neglected, it can be approximately obtained
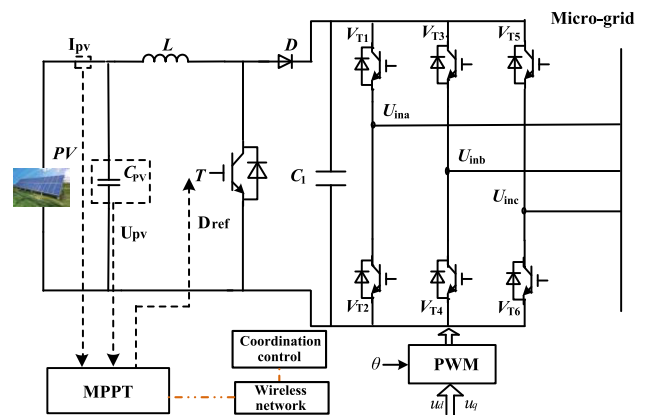

FIGURE 4. Configuration of a PV generation unit connected to the micro-grid.

that $P_{PV} = P_g = 3V_g I_g$, where V_g and I_g are indicated as the phase voltage and the phase current, respectively.

When the micro-grid meets the short-circuit fault, a voltage drop is usually followed to affect the renewable energy sources. If the behaviors of the PV are reasonably controlled, it can play a positive effect on the micro-grid in return. During the fault, the grid-side power is reduced from P_g to P_{gf}, and it is assumed that the DC/DC converter carries on transmitting the maximum power of the PV generation unit into the DC-link. The mathematical equation of the DC-link capacitor can be expressed as:

$$(P_{PV} - P_{gf})\Delta t = P_{DC1}\Delta t = \frac{1}{2}C_{DC1}(V_{DC1-f}^2 - V_{DC1}^2)$$
$$(7)$$

where V_{DC1} and V_{DC1-f} indicate the voltage over the DC-link capacitance before and after the fault, and Δt is the fault duration. Based on (7), V_{DC1-f} can be expressed as:

$$V_{DC1-f} = \sqrt{\frac{2(P_{PV} - 3V_{gf}I_{gf})\Delta t}{C_{DC1}} + V_{DC1}^2} \qquad (8)$$

In light of (8), the voltage drop under the fault enables to cause the power imbalance between P_{PV} and P_{gf}, and a high-amplitude overvoltage may be induced at the DC-link capacitance. One possible solution is to disable the maximum power point tracking control, and the decrease of the power P_{PV} can help to mitigate the power imbalance and avoid the capacitance damage. In addition, the voltage source inverter of the PV is able to offer the reactive current support based on different voltage drop levels. By referring to [26], the reference of the reactive current $I_{qpv-ref}$ is written as:

$$I_{qpv-ref} = I_n \times \frac{I_q}{I_n}$$
$$= \begin{cases} 0 & (0.9\text{pu} \leq V_{PV} \leq 1.1\text{pu}) \\ I_n(a - aV_{PV}) & (0.5\text{pu} \leq V_{PV} \leq 0.9\text{pu}) \\ I_n & (V_{PV} < 0.5\text{pu}) \end{cases} \quad (9)$$

where a is constant with the value of 2; V_{PV} is marked as the PV voltage; I_n is marked as the inverter's rated current.

The reference of the active current $I_{dpv-ref}$ is controlled as the following equation:

$$I_{dpv-ref} = \begin{cases} I_n & (0.9\text{pu} \leq V_{PV} \leq 1.1\text{pu}) \\ \sqrt{I_n^2 - I_{qpv-ref}^2} & (0.5\text{pu} \leq V_{PV} \leq 0.9\text{pu}) \\ 0 & (V_{PV} < 0.5\text{pu}) \end{cases} \quad (10)$$

Furthermore, the references of the active and reactive power are signified as:

$$\begin{cases} P_{ref} = 3V_g I_{dpv-ref} \\ Q_{ref} = 3V_g I_{qpv-ref} \end{cases} \qquad (11)$$

Based on the aforementioned analysis, FIGURE 5 shows the control block diagram of the voltage source inverter of the PV unit.
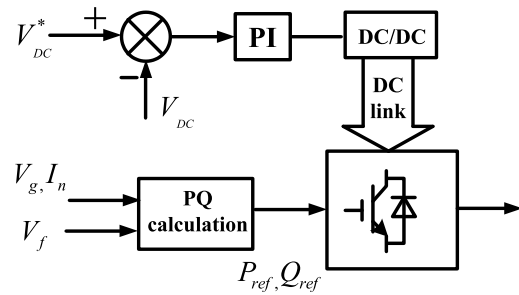

FIGURE 5. Control block diagram of the voltage source inverter of the PV unit.

D. BASIC COORDINATION PRINCIPLES FOR THE SMES, SFCL AND PV

In respect to the SMES, active SFCL and PV, the coordination control's basic principles for them in the micro-grid are defined as:

(1) When some severe or permanent faults occur, the micro-grid should be separated from the main network, due to the fact that it might lose the ability to provide a stable power exchange under serious or persistent voltage dips, and the coordination is to drive the micro-grid to be separated smoothly and reliably. In accordance with the determined fault types, the coordination center will activate the SMES to achieve the switching from its P-Q control to V-F control, drive the active SFCL to operate in the current-limiting mode 3, and make the distributed generation units take part in the voltage-frequency regulation. Since the most of distributed generation units are undispatchable dispersed sources, they may appreciatively use virtual synchronous generator technologies or change their original power tracking modes to participate in the stability control [27]–[29].

(2) When some minor or temporary faults happen, the coordination aims to assist the micro-grid to realize the fault ride-through (FRT) operation, so as to reinforce power support when the voltage dip is within an acceptable level. In light of the determination of fault severity, the coordination center will make the SMES maintain the original P-Q control, make the active SFCL operate in the current-limiting mode 1, and let the distributed generation units keep the maximum power point tracking control. As the fluctuations of the current and voltage under minor or temporary faults might have certain restricted margins, the coordination control enables to ensure the micro-grid's transient stability by use of this moderate control of the SMES, SFCL and distributed generation units.

In a way, the proposed coordination control is based on a heuristic approach. Nevertheless, the cooperation of the SMES, active SFCL and distributed generation units is systematically taken into account, and even the static power load can be regarded as taking part in the power adjustment due to that the voltage over it is compensated by the SFCL. In fact, no matter the severe fault or the minor fault, there will be a transient process in which the coordinating roles of the SMES, active SFCL and distributed generation units are all utilized. For the severe fault, the transient process

indicates the time range after the fault and before the micro-grid being separated, and for the minor fault, the transient process denotes the time range of fault ride-through. In the following, a brief discussion on how the SMES, active SFCL and distributed generation units cooperate to keep the power balance is presented.

Under normal state, the power balance of the micro-grid is:

$$P_{PV1} + P_{PV2} + P_{SMES} = P_{Load1} + P_{Load2} + P_{ex} \quad (12)$$

where P_{ex} is the exchange power between the micro-grid and the main network. As the active SFCL shows a low impedance in normal state, its power loss is ignored in this equation.

For that the fault occurs, the caused PCC voltage sag will directly reduce the power load and the exchange power, which are denoted as $P_{Load1-f}$, $P_{Load2-f}$, P_{ex-f}, respectively. Owing to the activation of the active SFCL, it starts to mitigate the PCC voltage drop and leads to the increase of the power load and the exchange power, which are marked as $P'_{Load1-f}$, $P'_{Load2-f}$, P'_{ex-f}, respectively. At the same time, the active SFCL can contribute to dissipating the surplus power from the micro-grid towards the main network, and this power is P_{SFCL}. Hence, the power equation of the micro-grid under the fault is rewritten as:

$$P_{PV1} + P_{PV2} + P_{SMES} = P_{SFCL} + P'_{Load1-f} \\ + P'_{Load2-f} + P'_{ex-f} \quad (13)$$

As $P_{SFCL} + P'_{Load1-f} + P'_{Load2-f} + P'_{ex-f} > P_{Load1-f} + P_{Load2-f} + P_{ex-f}$, the existence of the active SFCL can obviously relieve the pressure of the SMES and distributed generation units to deal with the power unbalance. Concerning the severe fault, the distributed generation units switch to the non-MPPT control, and the coordination center may acquire a specific power vacancy to determine the power reference for the SMES. Regarding the minor fault, there may be a restricted power vacancy, so the distributed generation units retain the original control and the SMES is to realize the power stabilization.

In light of the aforementioned description, FIGURE 6 shows the basic principles of the control switching under different operation conditions.

E. WIRELESS COMMUNICATIONS AND BRIEF ANALYSIS

In regard to building a data communication network for the micro-grid, the main reason is to achieve the data exchange among the coordination center and the SMES/SFCL/ distributed generation/loads. Wireline and wireless network architectures are two candidates. From the literature [30]–[32], when the micro-grid includes multiple distributed generation units, power loads and other controllable devices, a WiFi or ZigBee based wireless network may have better technical and economic performances than a fiber-optic wireline network, and the wireless network can serve the natural purpose of the micro-grid due to its great flexibility and low deployment cost. For the preliminary design of the wireless architecture, FIGURE 7 shows the network topology
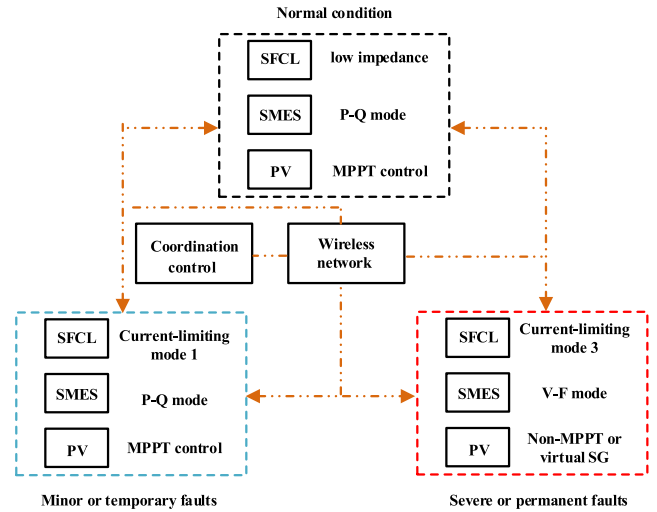

FIGURE 6. Basic principles of the control switching under different conditions. Note: MPPT control indicates maximum power point tracking control, and virtual SG denotes virtual synchronous generator.
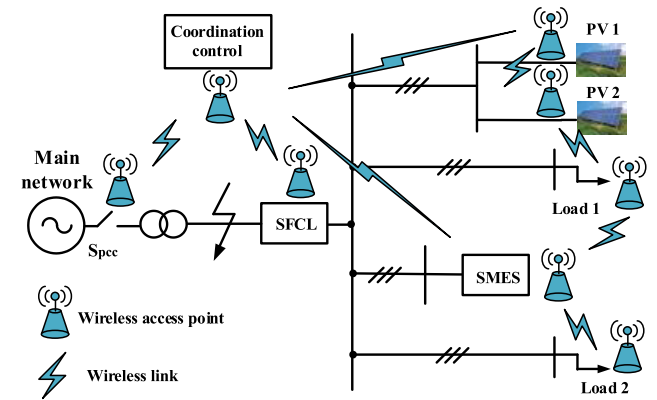

FIGURE 7. Network topology designed for the micro-grid's wireless communications.

designed for the micro-grid's wireless communications. Each of the micro-grid equipment or those major devices may configure a wireless access point, and thus the bidirectional and unidirectional wireless links between the APs can be formed.

To ensure this information interaction has higher generality, reliability, and scalability, the IEEE 802.11 based wireless network standard can be adopted [33], [34]. For classifying the information messages broadcasted in the wireless network, two types of key information messages are defined:

1) Status information, which is to describe the status of the individual element or the entire micro-grid, such as normal or faulted condition, open or closed status of the switch located at the point of common coupling (PCC).

2) Control information, which exists between the coordination center and the controllable devices. For the SMES or the SFCL, this control information should be the mode switching command. For the distributed generation units, it may be the power regulation command or the mode switching command.

In other words, the original maximum power point tracking may become invalid.

The control feedback is also needed. In the case of a communication failure, the individual element should have the ability to perform the presupposed function after a time delay based on local information, and this self-operation's priority level will be inferior to the coordination control.

III. SIMULATION STUDY
A. SYSTEM MODELING
The simulation model of the micro-grid with the SMES, active SFCL and distributed generation units is built in MATLAB/Simulink, and the validity of the suggested coordination control is assessed. The main simulation parameters are given in Table 1.

TABLE 1. Simulation parameters of the model.

Micro-grid with SMES, SFCL and distributed generation units	
PV1 / PV2	150 kW / 80 kW
Power Line	0.27+j0.347 Ω/km, 2 km
Nominal Load 1 / 2	60 kW / 40 kW
Nominal Voltage / Frequency	10 kV / 50 Hz
SMES Magnet	150 kJ / 100 kW
SMES Chopper	800 V / 5000 uF
Active SFCL	L_{s1}=80 mH, L_{s2}= 80 mH, M_s=72 mH

Note that, the PV1/PV2 uses the P-Q control and achieves the max output under normal state, and in the case of some severe or permanent faults, the original maximum power point tracking can be replaced by the non-maximum power point tracking, so as to conduct the self-protection and participate in the power regulation. For the modeling of the PV generation unit, please refer to [35] for more details.

The modeling of the static power load in the simulation analysis is based on a resistor element model, and the power equation can be expressed as $P_{\text{load}} = 3U^2/R$, where U is the phase-voltage over the resistor element, and R *is* the resistance value of the resistor element.

In respect to the modeling of the SMES, the voltage source converter and the chopper use the standard models from MATLAB element library, and the superconducting magnet is represented by a non-resistive inductance model [36]. For the modeling of the SFCL, the air-core superconducting transformer is emulated by a non-resistive transformer, and a voltage source converter integrated with DC capacitor model is built for the converter.

The selection of the parameters of the SMES and SFCL can basically refer to [37] and [38], and a detailed optimal design of them will be introduced in other articles. Based on the theoretical analysis of the superconducting devices in Section II, Tables 2-3 show the specifications of the SMES magnet and the air-core superconducting transformer used in the SFCL,

TABLE 2. Specifications of the SMES magnet.

Structure parameters		Operation parameters	
Magnet height	210.6 mm	Magnet voltage	800 V
Coil number	18	Magnet current	165 A
Inner diameter	240 mm (Bi coil); 264 mm (YBCO coil)	Operation temperature	20 K
Outer diameter	396 mm	Magnet inductance	11.2 H
Tape length	7200 m	Central magnetic field	3.75 T

TABLE 3. Specifications of the superconducting transformer used in the SFCL.

Structure parameters		Operation parameters	
Structure type	Solenoid pancakes	Max-compensating voltage	5 kV
HTS tape	YBCO	Critical current	130 A
Tape width / thickness / critical current	8 mm 0.096 mm 200 A	Operation temperature	77 K
Inner diameter	88 mm	Current-limiting ratio	0.5
Outer diameter	154 mm	Coupling factor	0.9

respectively. It is expected to lay a preliminary foundation for the optimization study of the device parameters in the future.

B. SIMULATION OF NORMAL CONDITION
When the micro-grid system operates in its normal energy exchanging state, FIGURES 8-9 show the simulation results of the distributed generation power P_{DG}, exchange power P_{ex}, load power P_{load} and three-phase PCC voltage. Regarding this normal case, the active SFCL has no influence on the operation of the micro-grid, and the SMES can maintain the exchange power at the level of 250 kW. As the output of the distributed generation units is larger than the two local power load, the flow direction of the exchange power is from the micro-grid towards the main network. The external characteristic of the micro-grid is equivalent to a power source, whose voltage and frequency will be well supported by the main network.

C. SIMULATION OF SEVERE FAULT
For the description of a severe fault, a three-phase external short-circuit occurs in the main network at $t = 1$ s, and a small fault resistance with the value of $R_g = 0.5$ Ω is adopted. The PCC switch will open at 120 ms after the fault, and then the micro-grid operates in its islanded state. FIGURES 10-11 show the transient behaviors of the micro-grid without and with the coordination control.

When the coordination control is not applied, the micro-grid will only rely on itself to resist this external fault. The active SFCL is not used, and the SMES unit will passively
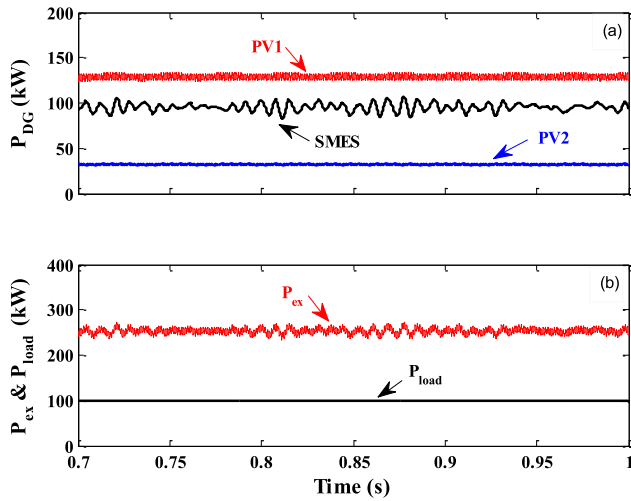
FIGURE 8. Operation behaviors of the micro-grid in normal condition. (a) Distributed generation power P_{DG}, (b) Exchange power P_{ex} & load power P_{load}.
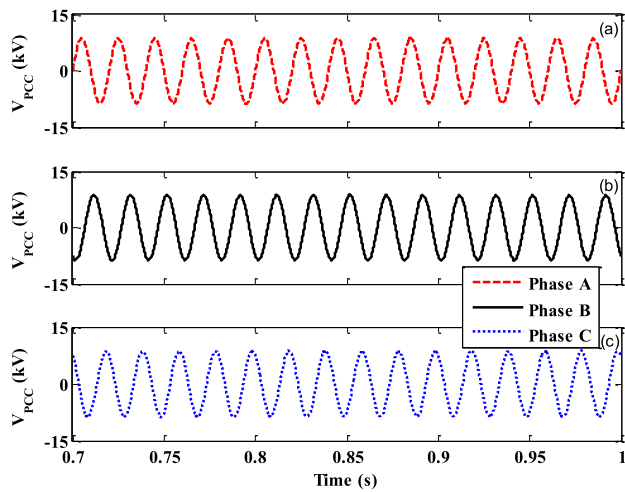

FIGURE 9. Three phase PCC voltage curves of the micro-grid in normal condition. (a) A-phase, (b) B-phase and (c) C-phase.

FIGURE 10. Power curves of the micro-grid in the case of a severe fault. (a) Distributed generation total power $P_{DG-total}$, (b) Load power P_{load} and (c) Exchange power P_{ex}.

FIGURE 11. Operation behaviors of the micro-grid in the case of a severe fault. (a) PCC current, (b) PCC voltage and (c) frequency response.

switch to the V-F control mode until the PCC switch finishes the separation from the micro-grid. As the PV units always running under MPPT, it may enlarge the power imbalance.

In the case of that the coordination control is utilized, the coordination center will drive the active SFCL and the SMES to play the corresponding roles, and the PV units can actively adopt the non-MPPT for reducing the power outputs. This is to protect the generation equipment and bring the SMES unit's initiative into full play. From the demonstrated figures, the coordination control of the SMES, SFCL and distributed generation units is able to offer the following contributions for the micro-grid: 1) Maintaining the power balance and accelerating the recovery of the load; 2) Suppressing the PCC fault current and compensating the PCC voltage sag; 3) Reducing the frequency fluctuation and improving the
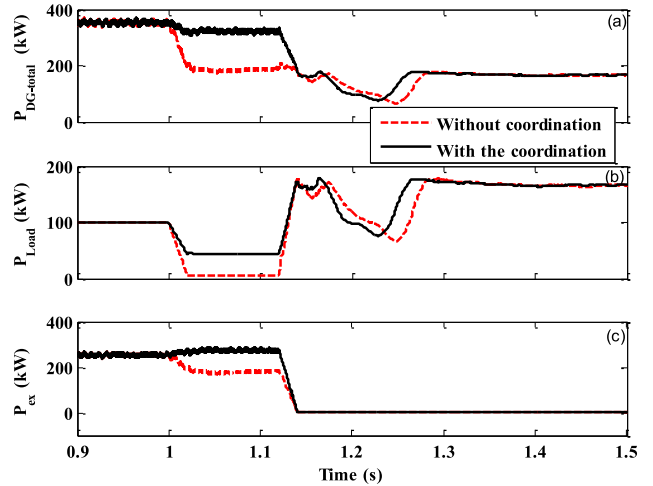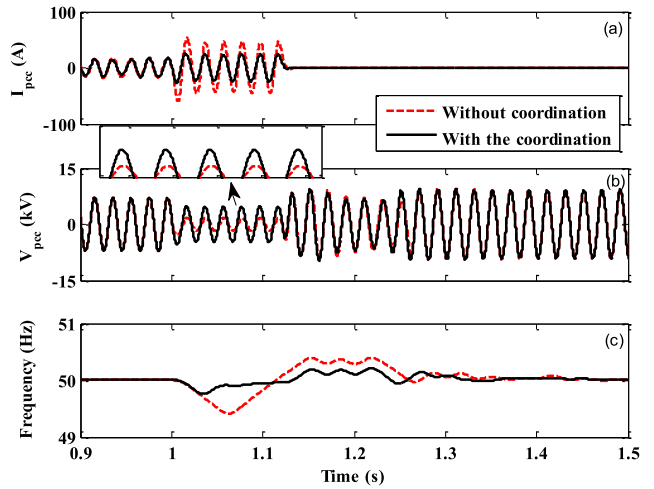
power quality. Table 4 shows the detailed performance comparison of with and without the coordination control.

Note that, when the micro-grid operates in the island mode, the V-F control of the SMES is activated to stabilize the voltage and frequency as much as possible. Nevertheless, there are still a certain control errors (optimizing control parameters may help to alleviate the errors), and the SMES may not completely make the micro-grid's voltage and frequency be constant before and after the mode switching. From the results, the PCC voltage under the islanded mode is increased to 1.28 times of the nominal voltage, and the power load raises to 166 kW not to its normal value (100 kW). For the total output of the distributed generation units, it is also adjusted to 166 kW, and thus a new power balance for the stable condition is achieved under the island mode of the micro-grid. Furthermore, considering that this kind of

TABLE 4. Performance of the micro-grid with and without the coordination.

Items	Transient performance indexes under the severe fault				
	Load power	Exchange power	Fault current	PCC voltage	Frequency fluctuation
Without coordination	7 kW	170 kW	50 A	1.74 kV	0.62 Hz
With the coordination	45 kW	270 kW	25 A	4.71 kV	0.28 Hz

unplanned mode transfer from grid-connected to island will generally have a short-term duration, the power load is able to timely recover to its nominal level after the re-connected operation is finished.

D. SIMULATION OF MINOR FAULT

For the simulation of a minor external fault, the increase of the fault resistance value is mainly taken into account. In this study, the three-phase external fault is still located near to the main network. The fault occurrence time and the fault resistance are set as $t = 1$ s and $R_g = 5$ Ω, respectively. After a duration of 120 ms, the minor external fault will be removed.

FIGURE 12 shows the operation behaviors of the micro-grid under the presupposed minor fault. Owing to the increase of the fault resistance, the transient fluctuations of the load power, PCC voltage and grid frequency will be mitigated as compared to the severe fault, and the coordination of the SMES, SFCL and distributed generation units can easy to assist the micro-grid to realize the FRT operation. There may be a critical fault resistance R_{gc} that is exactly out of the capability area of the coordination mode in accordance with the "minor" fault. Thus, the coordination mode for the "severe" fault will be applied to the case where the fault resistance is lower than R_{gc}.
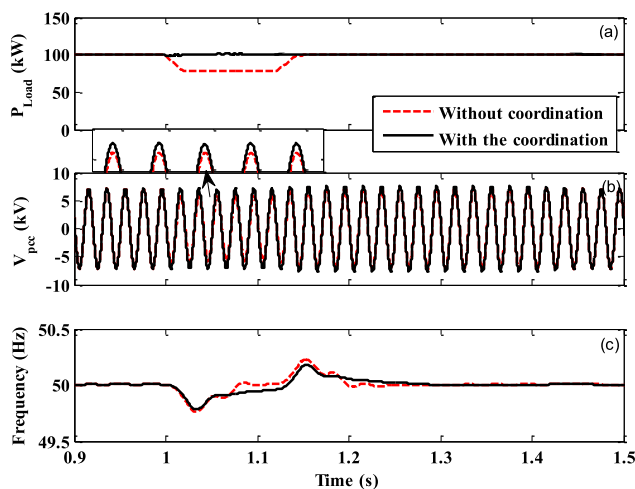

FIGURE 12. Operation behaviors of the micro-grid in the case of a minor fault. (a) Load power, (b) PCC voltage and (c) frequency response.

In view of that the micro-grid is coupled to the power distribution network rather than the power transmission

network, the fluctuation range of the fault resistance may be restricted. In respect to a severe fault with lower fault resistance, the value range of the fault resistance may be approximately set as 0∼2 Ω, and once an excessively higher fault resistance should be taken into consideration, its resistance value can be even set as 200 Ω [39]. In our simulation analysis, a simplified design of the critical fault resistance is that $R_{gc} = 2$ Ω.

Considering both of the severe fault and the minor fault, FIGURE 13 shows the impacts of the coordination control on the dc-link overvoltage of the PV generation (PV1 is selected). Due to the introduction of the coordination, the fluctuation amplitude and duration of dc-link overvoltage are well mitigated. Thus, the whole fluctuation process is greatly smoothed, so as to protect the capacitor from the
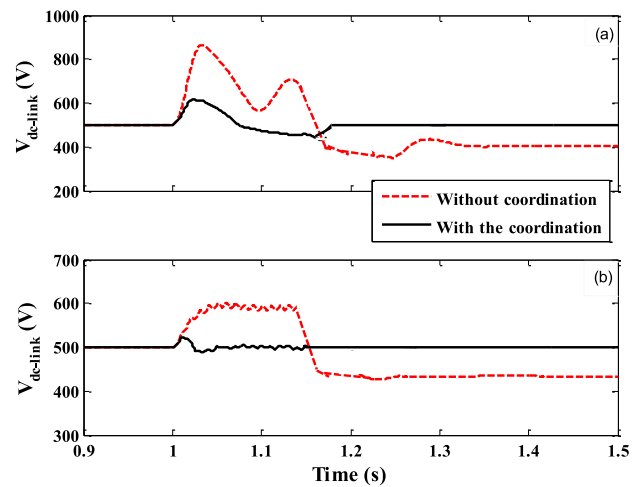

FIGURE 13. Impacts of the coordination control on the dc-link overvoltage of the PV1 under different faults. (a) Severe fault and (b) minor fault.
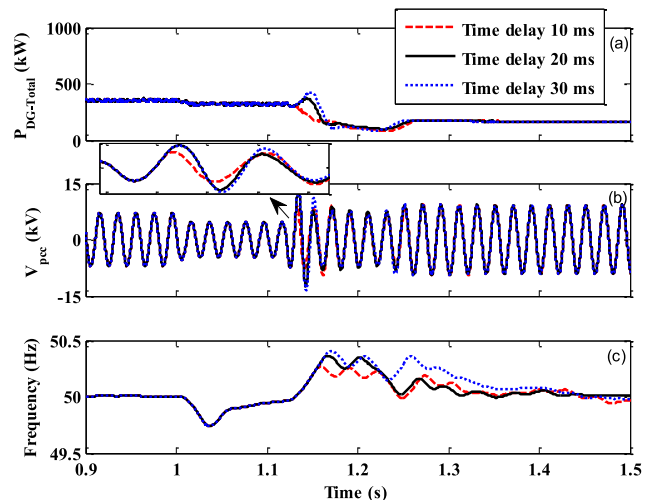

FIGURE 14. Impacts of different communication time delays on the micro-grid's performance in the case of a severe fault. (a) Distributed generation total power $P_{DG-total}$, (b) PCC voltage and (c) frequency response.

overvoltage surge. The simulation results agree with the theoretical analysis, and strengthening the safety and stability of the PV generation is helpful to the micro-grid.

E. SIMULATION OF COMMUNICATION DELAY

In this section, different communication time delays in the wireless network are also taken into account, and the related influence on the SMES unit's control switching is studied for the severe external fault ($R_\mathrm{g} = 0.5\ \Omega$).

FIGURE 14 shows the operation characteristics of the micro-grid under different communication delays, and it is noted that the decrease of time delay can ensure the coordination capability. Some follow-up works can be carried out to improve the wireless network's robustness against the communication failures and disturbances.

IV. CONCLUSION

In order to improve the stability of a micro-grid under short-circuit faults, this paper proposes and investigates the coordination of a SMES unit, an active SFCL, and multiple distributed generation units via the wireless communications. The severe and minor faults are considered, and the impacts of the wireless communication delay on the coordination performance are also studied. The results well demonstrate the effectiveness of the proposed coordination control, and it can maintain the power balance, accelerate the load recovery, suppress the PCC fault current, and mitigate the voltage-frequency fluctuation. Thus, the micro-grid's transient performance is able to be enhanced considerably, and further the technical advantages of the SMES, active SFCL, distributed generation units and wireless communications can be fully utilized.

In the near future, the improvement of the coordination control will be carried out from multiple aspects, such as the parameter optimizations of the SMES and the SFCL, the robustness advancement of the wireless network, the suitableness enhancement of the coordination control for a large micro-grid/test system including several DG resources and control structures. In addition, the current coordination control does not consider the effects of the load dynamics on the transient performance of the micro-grid, and it means that just two static power loads are used. On the one hand, with regard to the necessity of introducing the load dynamics, it may closely depend on whether the current coordination control of the SMES, active SFCL and distributed generation units is enough to stabilize the micro-grid under the fault conditions. On the other hand, if more electrical devices take part in the coordination control, an intelligent coordination method based on multi-agent system technology can be properly applied. Related research results will be reported in later articles.

REFERENCES

[1] J.-Y. Yoon, S.-R. Lee, and I.-T. Hwang, "A quantitative analysis on future world marketability of HTS power industry," *IEEE Trans. Smart Grid*, vol. 4, no. 1, pp. 433–436, Mar. 2013.

[2] J. Li, Q. Yang, F. Robinson, F. Liang, M. Zhang, and W. Yuan, "Design and test of a new droop control algorithm for a SMES/battery hybrid energy storage system," *Energy*, vol. 118, pp. 1110–1122, Jan. 2017.

[3] M. Song *et al.*, "100 kJ/50 kW HTS SMES for micro-grid," *IEEE Trans. Appl. Supercond.*, vol. 25, no. 3, Jun. 2015, Art. no. 5700506.

[4] T.-T. Nguyen, H.-J. Yoo, and H.-M. Kim, "Applying model predictive control to SMES system in microgrids for eddy current losses reduction," *IEEE Trans. Appl. Supercond.*, vol. 26, no. 4, Jun. 2016, Art. no. 5400405.

[5] L. Chen *et al.*, "Comparison of superconducting fault current limiter and dynamic voltage restorer for LVRT improvement of high penetration microgrid," *IEEE Trans. Appl. Supercond.*, vol. 27, no. 4, Jun. 2017, Art. no. 3800607.

[6] P. Shamsi and B. Fahimi, "Stability assessment of a DC distribution network in a hybrid micro-grid application," *IEEE Trans. Smart Grid*, vol. 5, no. 5, pp. 2527–2534, Sep. 2014.

[7] M. H. Syed, H. H. Zeineldin, and M. S. E. Moursi, "Hybrid micro-grid operation characterisation based on stability and adherence to grid codes," *IET Gener. Transm. Distrib.*, vol. 8, no. 3, pp. 563–572, Mar. 2014.

[8] S. I. Gkavanoudis and C. S. Demoulias, "A control strategy for enhancing the fault ride-through capability of a microgrid during balanced and unbalanced grid voltage sags," *Sustain. Energy Grids Netw.*, vol. 3, pp. 1–11, Sep. 2015.

[9] L. Guo, Y. Feng, X. Li, C. Wang, and Y. Li, "Stability analysis and research of active damping method for DC microgrids," *Proc. CSEE*, vol. 36, no. 4, pp. 927–936, Feb. 2016.

[10] A. V. Jayawardena, L. G. Meegahapola, D. A. Robinson, and S. Perera, "Low-voltage ride-through characteristics of microgrids with distribution static synchronous compensator (DSTATCOM)," in *Proc. Australas. Univ. Power Eng. Conf. (AUPEC)*, Wollongong, NSW, Australia, 2015, pp. 1–6.

[11] I. Ngamroo and S. Vachirasricirikul, "Optimized SFCL and SMES units for multimachine transient stabilization based on kinetic energy control," *IEEE Trans. Appl. Supercond.*, vol. 23, no. 3, Jun. 2013, Art. no. 5000309.

[12] W. Guo, L. Xiao, and S. Dai, "Enhancing low-voltage ride-through capability and smoothing output power of DFIG with a superconducting fault-current limiter–magnetic energy storage system," *IEEE Trans. Energy Convers.*, vol. 27, no. 2, pp. 277–295, Jun. 2012.

[13] W. Guo *et al.*, "Overview and development progress of a 1-MVA/1-MJ superconducting fault current limiter-magnetic energy storage system," *IEEE Trans. Appl. Supercond.*, vol. 26, no. 3, Apr. 2016, Art. no. 5200905.

[14] L. Chen *et al.*, "Coordinated control of SFCL and SMES for transient performance improvement of microgrid with multiple DG units," *Can. J. Elect. Comput. Eng.*, vol. 39, no. 2, pp. 158–167, 2016.

[15] K. Gong, J. Shi, Y. Liu, Z. Wang, L. Ren, and Y. Zhang, "Application of SMES in the microgrid based on fuzzy control," *IEEE Trans. Appl. Supercond.*, vol. 26, no. 3, Apr. 2016, Art. no. 3800205.

[16] J. Shi, A. Zhou, Y. Liu, L. Ren, Y. Tang, and J. Li, "Voltage distribution characteristic of HTS SMES magnet," *IEEE Trans. Appl. Supercond.*, vol. 26, no. 4, Jun. 2016, Art. no. 5700705.

[17] S.-T. Kim, B.-K. Kang, S.-H. Bae, and J.-W. Park, "Application of SMES and grid code compliance to wind/photovoltaic generation system," *IEEE Trans. Appl. Supercond.*, vol. 23, no. 3, Jun. 2013, Art. no. 5000804.

[18] F. Jiao *et al.*, "Electromagnetic and thermal design of a conduction-cooling 150 kJ/100 kW hybrid SMES system," *IEEE Trans. Appl. Supercond.*, vol. 23, no. 3, Sep. 2013, Art. no. 5701404.

[19] L. Ren *et al.*, "The experimental research and analysis of a HTS SMES hybrid magnet," *IEEE Trans. Appl. Supercond.*, vol. 25, no. 3, Jun. 2015, Art. no. 4601605.

[20] L. Chen, C. Deng, F. Guo, Y. Tang, J. Shi, and L. Ren, "Reducing the fault current and overvoltage in a distribution system with distributed generation units through an active type SFCL," *IEEE Trans. Appl. Supercond.*, vol. 24, no. 3, Jun. 2014, Art. no. 5600305.

[21] L. Chen, F. Zheng, C. Deng, Z. Li, and F. Guo, "Fault ride-through capability improvement of DFIG-based wind turbine by employing a voltage-compensation-type active SFCL," *Can. J. Elect. Comput. Eng.*, vol. 38, no. 2, pp. 132–142, Jun. 2015.

[22] D. Hu *et al.*, "A numerical method for calculating and optimizing the coupling factor of HTS air-core transformer," *IEEE Trans. Appl. Supercond.*, vol. 26, no. 6, Sep. 2016, Art. no. 5501106.

[23] M. Song, Y. Tang, Y. Zhou, L. Ren, L. Chen, and S. Cheng, "Electro-magnetic characteristics analysis of air-core transformer used in voltage compensation type active SFCL," *IEEE Trans. Appl. Supercond.*, vol. 20, no. 3, pp. 1194–1198, Jun. 2010.

[24] J. Wang, L. Zhou, J. Shi, and Y. Tang, "Experimental investigation of an active superconducting current controller," *IEEE Trans. Appl. Supercond.*, vol. 21, no. 3, pp. 1258–1262, Jun. 2011.

[25] L. Chen, Y. Tang, J. Shi, Z. Li, L. Ren, and S. Cheng, "Control strategy for three-phase four-wire PWM converter of integrated voltage compensation type active SFCL," *Phys. C, Supercond.*, vol. 470, no. 3, pp. 231–235, Feb. 2010.

[26] W. Kou, D. Wei, P. Zhang, and W. Xiao, "A direct phase-coordinates approach to fault ride through of unbalanced faults in large-scale photovoltaic power systems," *Elect. Power Compon. Syst.*, vol. 43, no. 8, pp. 902–913, 2015.

[27] Q.-C. Zhong and G. Weiss, "Synchronverters: Inverters that mimic synchronous generators," *IEEE Trans. Ind. Electron.*, vol. 58, no. 4, pp. 1259–1267, Apr. 2011.

[28] S. M. Ashabani and Y. A. R. I. Mohamed, "A flexible control strategy for grid-connected and islanded microgrids with enhanced stability using nonlinear microgrid stabilizer," *IEEE Trans. Smart Grid*, vol. 3, no. 3, pp. 1291–1301, Sep. 2012.

[29] T. Zheng, L. Chen, T. Chen, and S. Mei, "Review and prospect of virtual synchronous generator technologies," *Automat. Elect. Power Syst.*, vol. 39, no. 21, pp. 165–175, Nov. 2015.

[30] H. Liang, B. J. Choi, W. Zhuang, X. Shen, A. S. A. Awad, and A. Abdr, "Multiagent coordination in microgrids via wireless networks," *IEEE Wireless Commun.*, vol. 19, no. 3, pp. 14–22, Jun. 2012.

[31] H. Liang, B. J. Choi, W. Zhuang, and X. Shen, "Stability enhancement of decentralized inverter control through wireless communications in microgrids," *IEEE Trans. Smart Grid*, vol. 4, no. 1, pp. 321–331, Mar. 2013.

[32] T. S. Ustun and R. H. Khan, "Multiterminal hybrid protection of microgrids over wireless communications network," *IEEE Trans. Smart Grid*, vol. 6, no. 5, pp. 2493–2500, Sep. 2015.

[33] L. Seno, S. Vitturi, and C. Zunino, "Analysis of Ethernet powerlink wireless extensions based on the IEEE 802.11 WLAN," *IEEE Trans. Ind. Inf.*, vol. 5, no. 2, pp. 86–97, May 2009.

[34] Y. Zhang, N. Ansari, and H. Tsunoda, "Wireless telemedicine services over integrated IEEE 802.11/WLAN and IEEE 802.16/WiMAX networks," *IEEE Wireless Commun.*, vol. 17, no. 1, pp. 30–36, Feb. 2010.

[35] P. Giroux, G. Sybille, C. Osorio, and S. Chandrachood, *100-kW Grid-Connected PV Array Demo Detailed Model; MathWorks File Exchange*. Natick, MA, USA: MathWorks, 2012.

[36] J. Zhu, X. Bao, B. Yang, P. Chen, Y. Yang, and M. Qiu, "Dynamic simulation test research on power fluctuation compensation using hybrid SMES of YBCO and BSCCO tapes," *IEEE Trans. Appl. Supercond.*, vol. 22, no. 3, Jun. 2012, Art. no. 5700404.

[37] X. Ying, "Review on superconducting fault current limiters," *South Power Syst. Technol.*, vol. 9, no. 3, pp. 1–9, Mar. 2015.

[38] Y. Liu, Y. Tang, J. Shi, X. Shi, J. Deng, and K. Gong, "Application of small-sized SMES in an EV charging station with DC bus and PV system," *IEEE Trans. Appl. Supercond.*, vol. 25, no. 3, Jun. 2015, Art. no. 5700406.

[39] R. Mohanty, U. S. M. Balaji, and A. K. Pradhan, "An accurate noniterative fault-location technique for low-voltage DC microgrid," *IEEE Trans. Power Del.*, vol. 31, no. 2, pp. 475–481, Apr. 2016.

HONGKUN CHEN was born in Huanggang, Hubei, China, in 1967. He received the B.S. and M.S. degrees in electrical engineering from Xi'an Jiaotong University, China, in 1988 and 1990, respectively, and the Ph.D. degree from Wuhan University, China, in 1998. From 2000 to 2003, he was a Post-Doctoral Research Fellow with the School of Electrical Engineering, Osaka University.

He is currently a Professor and the Vice President of the School of Electrical Engineering, Wuhan University. His research interests include power system stability, power quality assessment/mitigation, and smart grid.

GUOCHENG LI was born in Shantou, Guangdong, China, in 1996.

He is currently pursuing the B.S. degree in electrical engineering from Wuhan University, Hubei, China. He is to further his study with the School of Electrical Engineering, Wuhan University, as a Graduate Student, in 2018. His research interests include power system simulation, distributed generation, and superconducting power application.

XIN TIAN was born in Ezhou, Hubei, China, in 1982. He received the B.S. degree from the Department of Electronic Science and Technology, Huazhong University of Science and Technology, Wuhan, China, in 2004, and the Ph.D. degree from the Institute for Pattern Recognition and Artificial Intelligence, Huazhong University of Science and Technology, in 2010. From 2015 to 2016, he was a Visiting Faculty Member with the School of Electrical and Computer Engineering, Georgia Institute of Technology. He is currently an Associate Professor with the Collaborative Innovation Center of Geospatial Technology, School of Electronic Information, Wuhan University, China. His current research interests include image/seismic compression, dictionary learning, sparse coding, and computational imaging.

YING XU (M'13) was born in China in 1989. He received the B.S. degree in electrical engineering and automation and the M.E. and Ph.D. degrees in electrical engineering from the Huazhong University of Science and Technology (HUST), Wuhan, China, in 2011 and 2016, respectively.
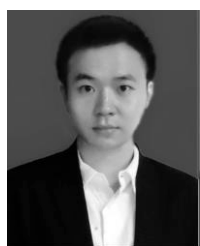
He is currently a Post-Doctoral Fellow with HUST. His research interests include applied superconductivity technology.

LI REN (SM'18) was born in China in 1968. She received the M.E. and Ph.D. degrees in engineering from the Huazhong University of Science and Technology (HUST), Wuhan, China, in 1990 and 2004, respectively.

She is currently a Professor with HUST, focusing on applied superconductivity technology.

LEI CHEN (M'12) was born in Jingzhou, Hubei, China, in 1982. He received the B.S. and Ph.D. degrees in electrical engineering from the School of Electrical and Electronic Engineering, Huazhong University of Science and Technology, Hubei, in 2004 and 2010, respectively.

From 2011 to 2013, he was with the Post-Doctoral Scientific Research Workstation, Hubei Electric Power Company. He is currently an Associate Professor with the School of Electrical Engineering, Wuhan University. He has authored over 80 articles. His research interests include power system simulation, smart grid, and superconducting power application.

YANHONG LI was born in Chengdu, Sichuan, China, in 1982. She received the B.S. degree in electrical engineering from the School of Electrical and Electronic Engineering, Huazhong University of Science and Technology, Hubei, in 2004, and the M.S. degree in electrical engineering from the School of Electrical Power, South China University of Technology, Guangzhou, in 2007.

She is currently a Senior Engineer with Guangzhou Power Supply Company Ltd., China Southern Power Grid Company Ltd. Her research interests include power system operation and analysis.

LIN ZHU (M'12) was born in Wuhu, Anhui, China, in 1982. He received the B.S. and Ph.D. degrees from the Huazhong University of Science and Technology, China, in 2005 and 2010, respectively. He was a Post-Doctoral Research Fellow with the Department of Control Science and Engineering, Huazhong University of Science and Technology.

He is currently a Research Assistant Professor with the Department of Electrical Engineering and Computer Science, The University of Tennessee, Knoxville. His main research interests include protective relaying and substation automation.

YUEJIN TANG received the B.S. and M.S. degrees in high-voltage engineering from the Huazhong University of Science and Technology (HUST), Wuhan, China, in 1982 and 1984, respectively, and the Ph.D. degree in engineering from Nagoya University, Nagoya, Japan, in 1996.

He is currently a Professor with HUST. His current research interests include applied superconductivity and high-voltage technology.

● ● ●